Infection, Genetics and Evolution 11 (2011) 1072–1082

Contents lists available at ScienceDirect

Infection, Genetics and Evolution

journal homepage: www.elsevier.com/locate/meegid

Research paper

Computational analysis and modeling the effectiveness of 'Zanamivir' targeting neuraminidase protein in pandemic H1N1 strains

Shailendra K. Gupta [a,d,1,*], Shishir K. Gupta [b], Suchi Smita [c], Mugdha Srivastava [b], Xin Lai [d], Ulf Schmitz [d], Qamar Rahman [c], Olaf Wolkenhauer [d], Julio Vera [d]

[a] Department of Bioinformatics, Indian Institute of Toxicology Research (CSIR), Lucknow, India
[b] Society for Biological Research & Rural Development, Lucknow, India
[c] Department of Bioinformatics, Integral University, Lucknow, India
[d] Department of System Biology & Bioinformatics, University of Rostock, 18057 Rostock, Germany

ARTICLE INFO

Article history:
Received 12 December 2010
Received in revised form 15 March 2011
Accepted 27 March 2011
Available online 2 April 2011

Keywords:
H1N1 Influenza virus
Swine flu
Antigenic drift
Neuraminidase
Zanamivir
Drug interaction
Mathematical model

ABSTRACT

Antigenic drift causes number of mutations in neuraminidase protein of H1N1 swine influenza virus. We analyzed neuraminidase mutations in H1N1 strains distributed over six continents, at both the sequence and structural level. Mutations in the nearby residues of the drug binding site play crucial role in the binding affinity of the drug with the protein. For this purpose, mutant models were generated for the neuraminidase protein from 34 pandemic H1N1 isolates and docking were performed with zanamivir drug. Multiple sequence alignment (MSA) and variations in docking score suggest that there are considerable changes in the binding affinity of neuraminidase with zanamivir, which leads to probable ineffectiveness of zanamivir in the isolated samples of pandemic H1N1 collected from quite a few countries. To further evaluate the effectiveness of the antiviral drugs, we derived, calibrated and analyzed an ordinary differential equations based mathematical model for H1N1 infection dynamics and drug mediated virus deactivation.

1. Introduction

Swine flu, one of the most treacherous diseases, is a respiratory ailment of pigs caused by type A influenza virus that could lead to complications such as bronchitis and pneumonia in human. Swine flu viruses have the capability to evolve continuously, when viruses from different species infect pigs, the virus undergoes reassortment and the new genome that was an example of triple reassortant from swine, avian and human influenza viruses (Wang and Palese, 2009). The H1N1 virus is contagious, spreading easily from one person to another and from one country to another. In the recent 2009 influenza pandemic, the H1N1 influenza virus causing the outbreak had evidently never been observed before and described as having components of human, avian and swine sources in its genome (Wang and Palese, 2009). Swine serve as a mixing-vessel (Webby et al., 2000), since they are susceptible to infection with viruses from birds and other mammals, thereby providing an opportunity for genetic reassortment between influenza viruses during a mixed infection (Altmuller et al., 1992). H1N1 are single-stranded, negative sense, segmented RNA viruses that belong to the family Orthomyxoviridae (Scholtissek et al., 1993). It is an enveloped RNA virus containing eight segments of negative-sense RNA (Webster et al., 1992), which encode 11 proteins, including hemagglutinin (HA), neuraminidase (NA), matrix 1 (M1), matrix 2 (M2), nucleoprotein (NP), nonstructural proteins (NS1 and NS2), and a polymerase complex (PA, PB1, PB1-F2 and PB2) (Mesecar and Ratia, 2008). Influenza A virus is further classified into subtypes according to the sixteen serotypes of hemagglutinin (H1 to H16) and 9 serotypes of NA (N1 to N9) surface glycoprotein antigens. Out of two agonist surface proteins: the HA is the receptor-binding and membrane fusion glycoprotein and the NA is a receptor-destroying enzyme (Brown, 2000). Currently, variants of three predominant HA-NA combinations of causative influenza viruses (H1N1, H3N2, and H1N2) are circulating in different swine populations throughout the world (Olsen, 2002; Schweiger et al., 2002). Most of the swine influenza virus strains are susceptible to two FDA-approved drugs, oseltamivir phosphate (Tamiflu) and zanamivir (Relenza). NA was chosen as a suitable drug target as it plays a major role in influenza virus propagation (Burmeister et al., 1991; Taylor and Vonitzstein, 1994). Zanamivir is a NA inhibitor, with potent,

* Corresponding author at: Department of Bioinformatics, Indian Institute of Toxicology Research (Council of Scientific & Industrial Research), Post Box 80, MG Marg, Lucknow 226 001, India. Tel.: +91 522 2284591; fax: +91 522 2628227.
E-mail addresses: shailendra.gupta@uni-rostock.de, skgupta@iitr.res.in (S.K. Gupta).
[1] Tel.: +49 381 4987575; fax: +49 381 4987572.

1567-1348/$ – see front matter © 2011 Elsevier B.V. All rights reserved.
doi:10.1016/j.meegid.2011.03.018

specific antiviral activity, has been shown to be effective against a number of strains of influenza tested, including those which shows the resistance to oseltamivir. It is found to be effective against wide range of influenza A and B viruses both in vitro and in laboratory animals by preventing release of progeny virions budding out from cell surface (Ferraris et al., 2005; Colman, 1999; Barnett et al., 2000). Administration by inhalation results in direct delivery to the respiratory tract, the principal site of viral replication (Monto et al., 2000). Mutation in a nearby residue of the drug binding site plays a vital role in the binding affinity of the drug with the corresponding protein. Random mutation and single amino acid substitution in HA and NA proteins causes antigenic drift and occurs during viral replication (Scholtissek et al., 1993). The ability of influenza virus to undergo continuous and progressive amino acid change may also cause an inappropriate binding of the drug. Variation in binding sites may block drug binding domains. The H274Y NA mutation in H1N1 resulted in reduced sensitivity in oseltamivir, also the H274N point mutation gave resistance to zanamivir (Ives et al., 2002). Hurt et al. (2009) have analyzed Gln136Lys neuraminidase mutation that caused approximately 300 fold-reduction of zanamivir susceptibility. Wang and co-workers also reported alteration in the sensitivity for both oseltamivir and zanamivir in the influenza A/WS/33 (H1N1) virus variant carrying a His274Tyr mutation in the NA protein. Other mutations, such as His274Gly, His274Ser, His274Asn and His274Gln were also shown to reduced sensitivity to zanamivir (Wang et al., 2002). As the human influenza strains are repeatedly evolving via these point mutations, the virus is able to escape from the limited antibody repertoire of the human immune response. Antigenic drift rate is sufficiently high in HA and NA and enough to create several antigenic variants each year (de Jong et al., 2007). Monitoring antiviral susceptibility is required to take account of the probable emergence of drug-resistant variants. As zanamivir is the only approved potential drug therapy in case of oseltamivir-resistant viral variants, detail investigation to analyze all the circulating mutations in NA that can result in the change in drug susceptibility is of enormous importance. In the present work, we analyzed the NA protein variants of H1N1 collected from all 6 continents for possible drift in the zanamivir binding domain and its impact on drug resistibility in the virus. A mathematical model was also derived and calibrated which consists of a series of ordinary differential equations (ODE) describing the drug mediated virus deactivation and the dynamics of the infectious process.

2. Materials and methods

2.1. Sequence collection

With the intention of analyzing mutation pattern in pandemic H1N1 NA protein, sequences were retrieved from the EpiFlu database (http://platform.gisaid.org/). We selected sequences covering 86 countries from all 6 continents for global mutational analysis. We collected all the NA protein sequences submitted in the database, and selected one representative sequence from each country (Supplementary Table 1) as we did in our previous work (Gupta et al., 2010).

2.2. Structural analysis of 1918 H1N1 neuraminidase complex with zanamivir

For the structural analysis of the binding site, the crystal structure of neuraminidase A/Brevig Mission/1/1918 H1N1 strain

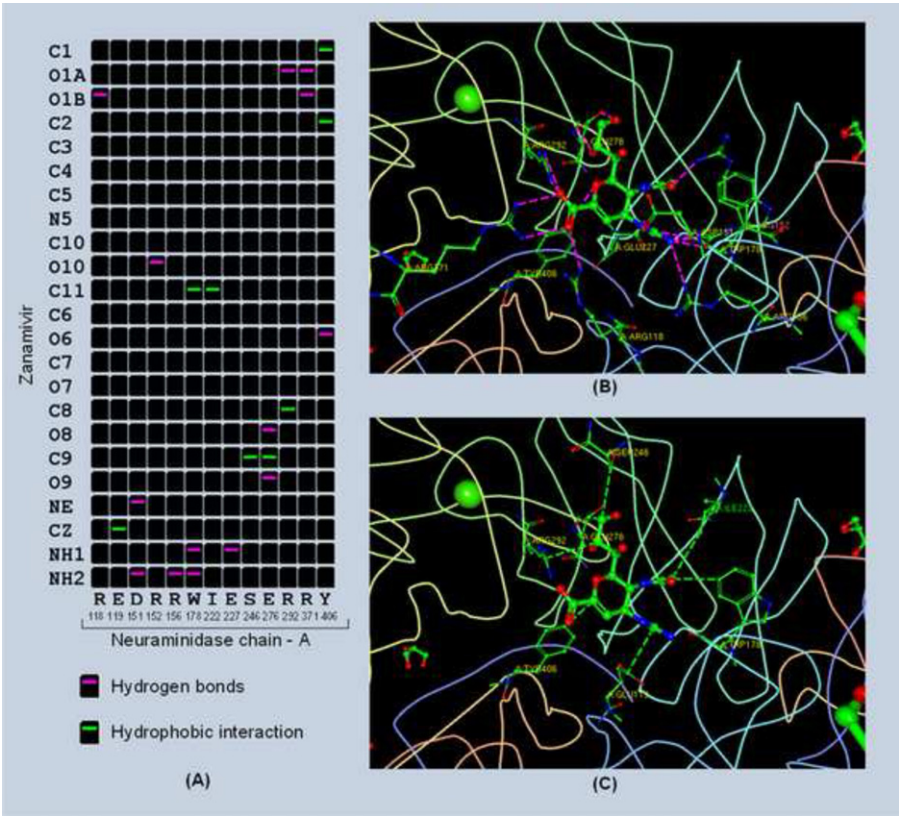

Fig. 1. Interaction of zanamivir drug with the NA protein of 1918 H1N1. (A) Contact map between different atoms of zanamivir with that of amino acid residues in the binding cavity of NA. (B) Hydrogen bonds (pink dashed lines) and (C) hydrophobic interactions (green dashed lines) of drug with amino acid residues are shown. All amino acid residues involved in the interactions are labeled. (For interpretation of the references to color in this figure legend, the reader is referred to the web version of the article.)

(Xu et al., 2008) in complex with zanamivir (PDB id: 3B7E) was selected from protein data bank. Binding site residues information of 3B7E with regard to zanamivir was extracted using PDB Ligand Explorer (Fig. 1).

2.3. Sequence alignment

Multiple sequence alignment (MSA) of all 86 sequences collected from all six continents and 1918 pandemic H1N1 NA protein (Swiss-Prot id: Q9IGQ6) was performed using the ClustalX 2.0.11 (Larkin et al., 2007). Redundant sequences with 100% similarity were removed using the redundancy removal protocol of the Jalview software (Waterhouse et al., 2009). To locate mutant amino acid residues positions in the remaining H1N1 NA protein sequences, pairwise alignments with the 1918 H1N1 neuraminidase protein sequence (Swiss-Prot id: Q9IGQ6) were performed using the matcher program of mEMBOSS 6.0.1 (Rice et al., 2000), with BLOSUM62 scoring matrix, gap opening and extension penalty 14 and 4 respectively.

2.4. Mutation modeling

All amino acid residues in the non-redundant sequence dataset were analyzed for any possible mutations using pairwise alignment with the sequence of 1918 H1N1 NA protein. In order to analyze the impact of single point mutation in the sequence data collected, equal weightage were given for each mutation site irrespective of amino acid residue type. For the mutant modeling, several homologous structures identified from PDB (3B7E, 3BEQ, 1A4G, 1A4Q, 3CL2, 2HTQ, 2HT7, 2HT8, 3CKZ, 3CL2 and 2HU4), Neuraminidase of A/Brevig Mission/1/1918 H1N1 strain in complex with zanamivir (PDB ID: 3B7E) were selected as the best template based on GA341 score function (Eramian et al., 2006) and protein sequence similarity. Total 10 confirmations of mutant model were generated for all the non-redundant sequences. We used the "Build Mutant" protocol of Accelrys Discovery Studio that automatically mutates specific residues and optimizes the confirmation of neighboring residues that lie within a specified cutoff radius of 4.5 Å. The protocol as described by Feyfant and co-

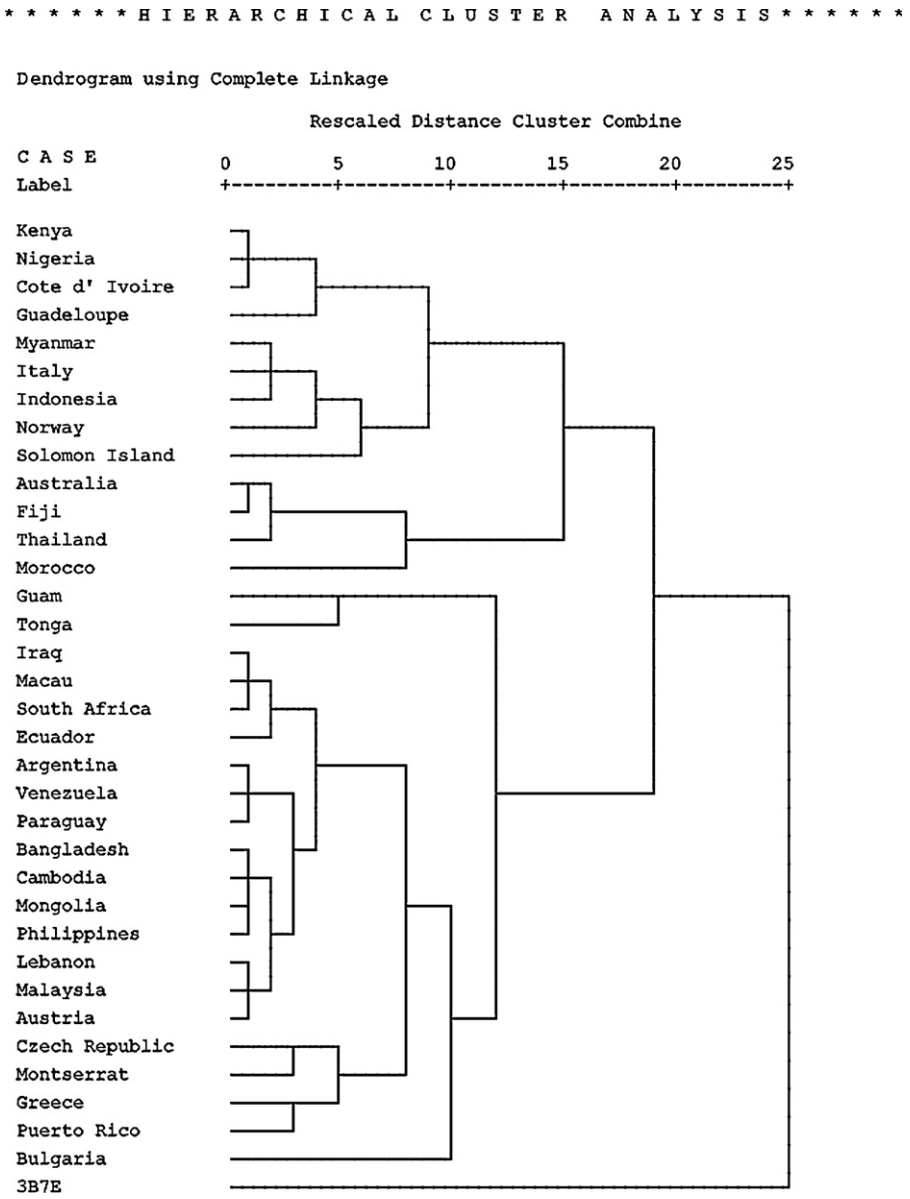

Fig. 2. Hierarchical clustering of NA protein from 34 representative countries / groups with 1918 H1N1 NA (PDB id: 3B7E) sequence, based on DOPE score; PDF Total Energy and pairwise alignment score. *G1 to G9 represents Groups shown in Table 1.

workers optimizes all the atoms of mutated residues using a scoring function which includes molecular mechanics energy terms for bond distances; bond angles; dihedral angles; peptide bond planarity; Lennard–Jones potential for non-bonded interaction; homology derived restraints for main-chain and side-chain dihedral angles; and statistical potential for non-bonded atom interactions extracted from large set of known protein structures (Feyfant et al., 2007). All the mutant models were further energy minimized in order to relax the conformation and remove the steric overlap that produces bad contacts for 400 steps of "Steepest Descent" minimization followed by 1000 steps of "Conjugated Gradient" minimization with CHARMm force field using "Minimization" protocols.

2.5. Model evaluation

All mutant model structures were evaluated using DOPE scoring functions and PDF Total Energy. The DOPE score of a protein can be viewed as a conformational energy which measures the relative stability of a conformation with respect to other conformations of the same protein. It can assist in choosing the best model out of a set of predicted model structures of a protein sequence. PDF Total Energy is the sum of the scoring function value of all homology-derived pseudo-energy terms and stereo-chemical pseudo-energy terms (Shen and Sali, 2006). Structures with lowest DOPE score and PDF Total Energy were selected for individual mutant model. For all the developed mutant models, hierarchical clustering was performed using SPSS v14.0 considering three parameters (1) alignment score by matcher with wild type NA protein sequence; (2) DOPE score and (3) PDF Total Energy of individual model (Fig. 2). All the generated models were also superimposed to analyze root mean square deviation (RMSD) in the structure.

2.6. Molecular docking

"Dock Ligands (LigandFit)" protocol in Discovery Studio (Accelrys, San Diego, CA) was used to analyze the impact of mutations on the binding affinity of zanamivir in the same binding cavity as it was in Neuraminidase of A/Brevig Mission/1/1918 H1N1 strain (PDB ID: 3B7E). A maximum of 10 poses of zanamivir were generated in the binding cavity of each mutant models. These poses were ranked according to DockScore [= −(ligand/receptor interaction energy + ligand internal energy)], Piecewise Linear Potential 1 (Gehlhaar et al., 1995), Piecewise Linear Potential 2 (Gehlhaar et al., 1999), LigScore 1 and LigScore 2 (Krammer et al., 2005), Potential of Mean Force (Muegge and Martin, 1999) and Jain (Jain, 1996) empirical scoring function. Accordingly, based on the binding efficacy of zanamivir with mutant models, the strains were grouped as susceptible strains (SS); partially drug-resistant strains (PRS) and fully drug-resistant strains (RS).

2.7. Mathematical modeling

In order to evaluate the effectiveness of the antiretroviral drug zanamivir in different strains of H1N1, we derived, calibrated and analyzed a mathematical model for the H1N1 infection. A schematic representation of the model appears in Fig. 3. Here, the process of infection, the immune response and the effect of drugs are represented in a simplified manner. We notice that drugs are external independent regulators of the system, while the immune response constitutes a delayed saturated-like feedback-loop system. In order to derive our model in ordinary differential equations, previously published models (Bocharov and Romanyukha, 1994; Beauchemin et al., 2005; Baccam et al., 2006; Alexander et al., 2008) developed to investigate similar infection systems

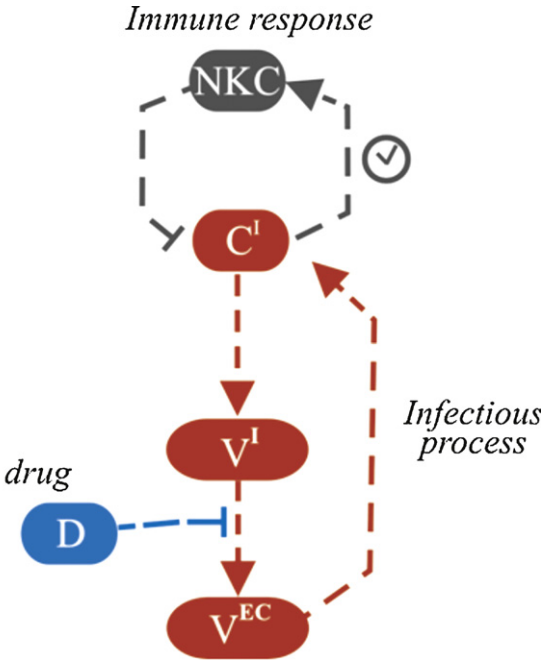

Fig. 3. Sketch of the model describing the process of infection, the immune response and the effect of antiviral drugs. NKC accounts for natural killer cells, C^I for population of infected cells in the nasal epithelium, V^I for the population of intracellular viruses, V^{EC} for the fraction of extracellular infection-active viruses and D for the concentration of drug.

were retrieved, modified and extended to construct our model. The result is an ODE model in kinetic rate equations (Fig. 4) with five differential equations describing the critical steps in the processes of virus infection and drug-mediated virus deactivation and its effect on the dynamics of the infectious process. Variables included in the model are: population of intracellular viruses (V^I), population of extracellular viruses (V^{EC}) capable of infecting new cells, population of deactivated viruses (V^B) after drug therapy, population of infected epithelial cells (C^I), population of

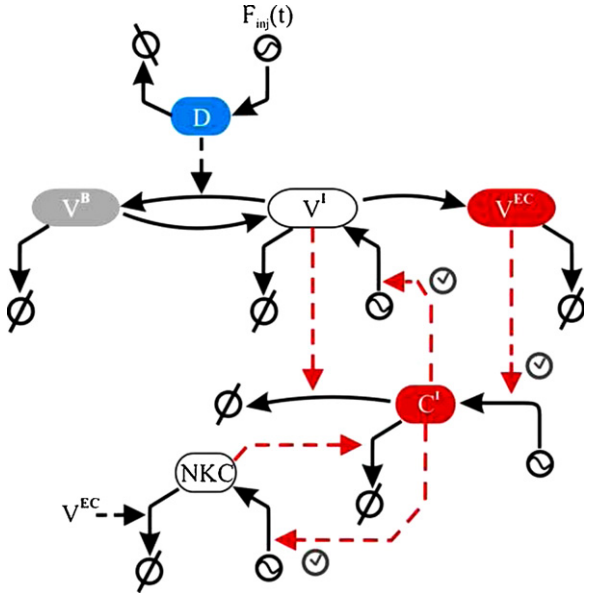

Fig. 4. Graphical representation of the ODE model describing the process of infection. Solid lines represent rate processes. The symbols ⊘ and ∅ refer to synthesis and degradation processes respectively. The "clock" symbol ⏲ refers to a time-delay in the considered process.

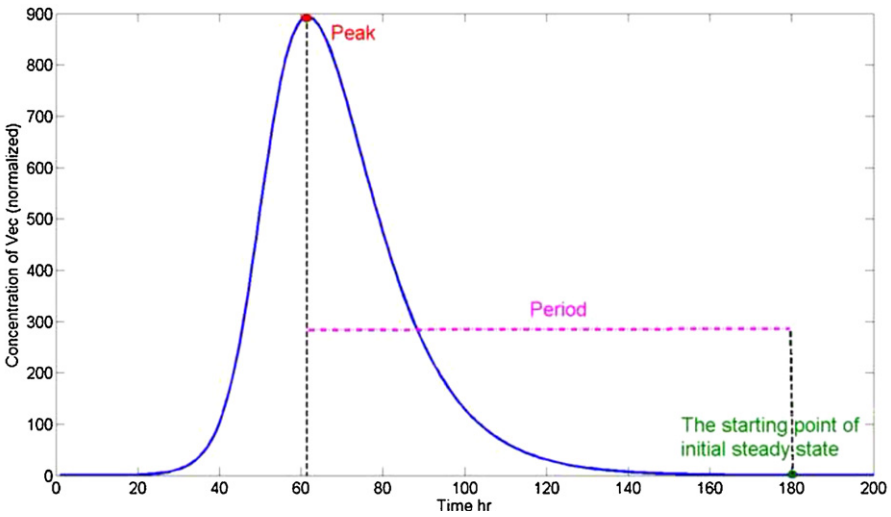

Fig. 5. Predictive simulations properties computed are; (1) intensity of peak of infection and (2) the duration of the infection.

recruited natural killer cells (NKC) and administration of drugs (D). In our model D was assumed to be a tunable time-dependent model parameter and for the sake of simplicity pharmaco-kinetics of the drug has not been included. The model focuses on the analysis of how specific mutations of NA proteins in different strains of the virus affect the efficacy of the treatment based on the administration of zanamivir. The ODE equations integrated with the mathematical model are described in Appendix A along with the list of parameters. The model was calibrated by using experimental data extracted from Baccam and coworkers under three different experimental conditions (Appendix B) concerning administration of zanamivir (Baccam et al., 2006).

2.8. Model simulation

The model was further used to perform a series of predictive computational simulations accounting for the effect of different zanamivir administration patterns to different patient populations concerning the strength of their immune system and the existence of mutations in the virus able to resist the drug therapy. Three conditions where simulations were performed are: SS; PRS; and RS. These three conditions were simulated by tuning the value of the parameter accounting for drug-virus binding k_{DB} ($SS: k_{DB} = k^0_{DB}, k_{RA} = k^0_{RA}$; $RS: k_{DB} = 0, k_{RA} = 0$; $PRS: k_{DB} = 0.1 \times k^0_{DB}, k_{RA} = k^0_{RA}$). For our simulations we further tuned the parameters accounting for delay in the administration of zanamivir ($\tau \in [0, 100]$ h) and the strength on the immune system in terms of efficient recruitment of natural killer cells ($k_{REC} \in [0.1, 10] \times k^0_{RECO}$). Predictive simulations for the dynamics of virus infection under the experimental conditions specified by tuned parameters were run in SBtoolbox2 for Matlab, and for each condition, the simulated intensity of peak and the duration of the infection were computed according to the description in Fig. 5.

3. Results

Analysis of binding interaction between 1918 H1N1NA with zanamivir (PDB id: 3B7E) showed that amino acid residues Arg118, Asp151, Arg152, Arg156, Glu227 and Arg371 were involved in hydrogen bond interactions; Glu119, Ile222 and Ser246 in hydrophobic interactions; while Trp178, Glu276, Arg292 and Tyr406 were participating in both hydrogen bond and hydrophobic interactions with the drug (Fig. 1). From the global sequence alignment of the 1918 H1N1 NA protein sequence with the NA from 2009 pandemic H1N1 isolates from all 6 continents, a total of nine groups/clusters were identified, having more than one sequence with 100% sequence similarity. The sequence data were grouped using redundancy removal protocol available in Jalview software. These groups along with country name are shown in Table 1 and cover 53 out of 78 sequences selected initially. The largest group (G8) contains 15 countries, distributed throughout the globe (Fig. 7).

Three dimensional structures of all 25 variants from different countries (with less than 100% sequence similarity) and 9 groups (represented as G1 to G9) were developed using 1918 H1N1 NA (PDB id: 3B7E) as a template structure. This structure is already used by several researchers for homology modeling followed by molecular dynamics simulation studies of different inhibitors targeting neuraminidase (Wang et al., 2010, 2009; Du et al., 2010). All 34 models (25 variants + 9 groups) were evaluated using DOPE score; PDF Total Energy and pairwise alignment score (Table 2) and the hierarchical clustering based on these parameters is depicted in Fig. 2.

RMSD matrix generated after structural superimposition based on C-alpha atom of all amino acid residues from 34 mutant models with 1918 H1N1 NA is shown in Supplementary Fig. 1. A total of 6 clusters with identical NA protein structures (RMSD 0.00) were identified after structure superimpositions. These includes (1) Mangolia, Bangladesh, Combodia; (2) Soloman Island, Indonesia; (3) Nigeria, Kenya, G3; (4) Malaysia, Lebanon; (5) Macau, Ecuador, Iraq; and (6) G1, G9.

All mutant structures were docked with zanamivir using "Dock Ligand (LigandFit)" protocol available in Accelrys Discovery Studio

Table 1
Isolates from different countries with identical NA protein sequence are grouped as G1 to G9.

Group	Representative countries
G1	Argentina, New Caledonia
G2	Bulgaria, Costa Rica, Egypt, Hungary, India, Kuwait, Latvia, Nicaragua, Peru, Romania, Slovakia, Slovenia
G3	Cote d'Ivoire, Russia
G4	Czech Republic, Nepal, Qatar
G5	Guadeloupe, China
G6	Guam, Panama
G7	Philippines, Brazil, Finland, French Guinea, Guatemala, Japan, Kazakhstan, Martinique, Taiwan, Vietnam,
G8	Thailand, Canada, Chile, Denmark, El Salvador, England, Germany, Israel, Mexico, Netherland, New Zealand, Portugal, South Korea, Sweden, USA
G9	Venezuela, Honduras, Singapore, Uruguay, Ukraine

Table 2
DOPE score, PDF physical energy and alignment score of mutant models with wild-type 3B7E.

Country	Dope score	PDF physical energy	Alignment score
G1	−45333.59	−10478.83	1901
G2	−45963.1	−10805.97	1918
G3	−45499.52	−9892.81	1918
G4	−45713.37	−10320.1	1918
G5	−45173.22	−9831.42	1900
G6	−45377.79	−10406.23	1893
G7	−45283.39	−10381.74	1898
G8	−44968.3	−10556.01	1959
G9	−45333.59	−10478.83	1900
Australia	−44924.77	−10510.12	1962
Austria	−45242.42	−10394.28	1897
Bangladesh	−45312.86	−10374.6	1901
Cambodia	−45312.86	−10374.6	1895
Ecuador	−45505.08	−10279.1	1913
Fiji	−44895.1	−10484.26	1926
Greece	−45853.44	−10574.78	1916
Indonesia	−44911.94	−10106.84	1909
Iraq	−45505.08	−10279.1	1917
Italy	−44849.1	−10013.34	1910
Kenya	−45499.52	−9892.81	1913
Lebanon	−45201.7	−10388.44	1917
Macau	−45505.08	−10279.1	1905
Malaysia	−45201.7	−10388.44	1919
Mongolia	−45312.86	−10374.6	1904
Montserrat	−45906.19	−10247.6	1895
Morocco	−44307.48	−10387.43	1914
Myanmar	−44794.01	−10080.57	1919
Nigeria	−45499.52	−9892.81	1902
Norway	−45077.55	−10212.6	1909
Paraguay	−45328.75	−10463.63	1913
Puerto Rico	−45624.7	−10519.92	2000
Solomon Island	−44911.94	−10106.84	1912
South Africa	−45571.83	−10312.41	1896
Tonga	−45194.23	−10562.29	1924

G1–G9 represents groups shown in Table 1.

Table 3
Comparison of binding affinity of zanamivir drug to the mutant models and 1918 H1N1 (3B7E) NA protein based on DockScore.

Strain type	Country	DockScore
Susceptible strain (SS)	Morocco	118.29
	Norway	108.546
	Indonesia	106.015
	Iraq	105.57
	Solomon Island	105.118
	G4	104.98
	Macau	104.887
	G7	104.386
1918 H1N1 NA	3B7E	104.029
Partially drug-resistant strain (PRS)	Australia	103.383
	G1	102.21
	G9	102.21
	Ecuador	102.1
	G8	102.068
	Austria	101.661
	Myanmar	101.028
	Italy	101.004
	Bangladesh	100.518
	Paraguay	100.351
	Peurto Rico	98.61
	Mongolia	96.655
	South Africa	95.021
	Cambodia	94.909
	Malaysia	93.168
	Lebanon	89.482
	Greece	81.232
	Tonga	79.078
	G6	73.035
Fully drug-resistant strain (RS)	G2	No ligand docked
	G3	No ligand docked
	G5	No ligand docked
	Fiji	No ligand docked
	Kenya	No ligand docked
	Montserrat	No ligand docked
	Nigeria	No ligand docked

G1–G9 represents groups shown in Table 1.

to indentify the impact of mutations in H1N1 NA protein on the binding affinity of zanamivir. The binding affinity is measured in the form of various empirical scoring functions. All the complexes are arranged in the descending order of DockScore (Table 3). DockScore of 1918 H1N1 NA and zanamivir was assumed as threshold value, above which the strains were enunciated as susceptible strains (SS) and below the threshold as partially drug-resistant strains (PRS) or full drug-resistant strains (RS).

Processes described in the dynamic model are concerning (i) virus dynamics: virus inoculation, virus infection-mediated proliferation, virus natural degradation, virus extracellular activation and virus deactivation by antiviral drugs targeting critical virus protein NA; (ii) epithelial cell population dynamics: cell turnover, virus mediated cell infection and natural killer mediated destruction; (iii) natural killer cells (NKC): infected cell mediated recruitment, virus mediated infection and destruction of NKC and NKC delocalisation after the end of the infection (Fig. 4).

Analysis of effectiveness of zanamivir on SS, PRS and RS are depicted in Fig. 6. For fully drug-resistant strains (Fig. 6C), administration of drugs does not affect the dynamics of infection, but the efficiency in the recruitment of NK cells do drastically affect the fate of the infectious process. In this way, the model suggests that for patients with a weak immune system ($k_{REC} \ll 1$), the infection may render critical both in the intensity of the viral charge reached at the peak and the duration of the infection and the condition may become fatal. In case of SS where the virus is susceptible to the drug (Fig. 6A), the model suggests that individuals with a healthy immune system may overcome the infection even in absence of treatment; in that case the early drug administration may reduce the intensity in the peak of infection. For individual with weak immune system, antiviral drugs may effectively mitigate the infection for early drug administration, but it may be insufficient to avoid intense viral charge in case of an excessive delay in the drug administration. Interesting enough, the simulations show a rather irregular pattern for the duration of the infection in the susceptible-type, with short recovery time for weak immune system and intermediate drug administration time and longer periods for extreme delay in the administration time. The most interesting situation happens for PRS to the antiviral drug (Fig. 6B). In this case, the simulations suggest that early drug administration help reducing the viral charge quicker in all the immune conditions, but may become insufficient with a long delay in drug administration in case of individuals with weak immune system. In this case, critical infectious conditions may be fulfilled for weak individuals and extremely delay in the drug administration (more than 72 h).

4. Discussion

Zanamivir works by binding with the viral protein NA and impeding the receptor perforation. Mutations in NA residues of H1N1 strains are so momentous that it may lead to ineffective or no binding of zanamivir with some mutants conferring resistance. Some of the current methods for monitoring drug resistance include phenotypic and genotypic analysis of neuraminidase gene, pyrosequencing (Bright et al., 2006), or flow cytometric analysis of virus-infected cells (McSharry et al., 2004), all of which are costly and time-consuming. Global surveillance coordinated by the in

silico studies have shown the evidence of considerable differences in the ability of resistance in isolates collected from different geographical regions. Some viruses with mutations may become resistant to the drug because of conformational rearrangement of residues around drug binding sites. Patients infected with such strains of the virus show resistance against the same drug and unknowingly spread the resistant strain globally when visiting several countries. Strict systematic monitoring of mutations in

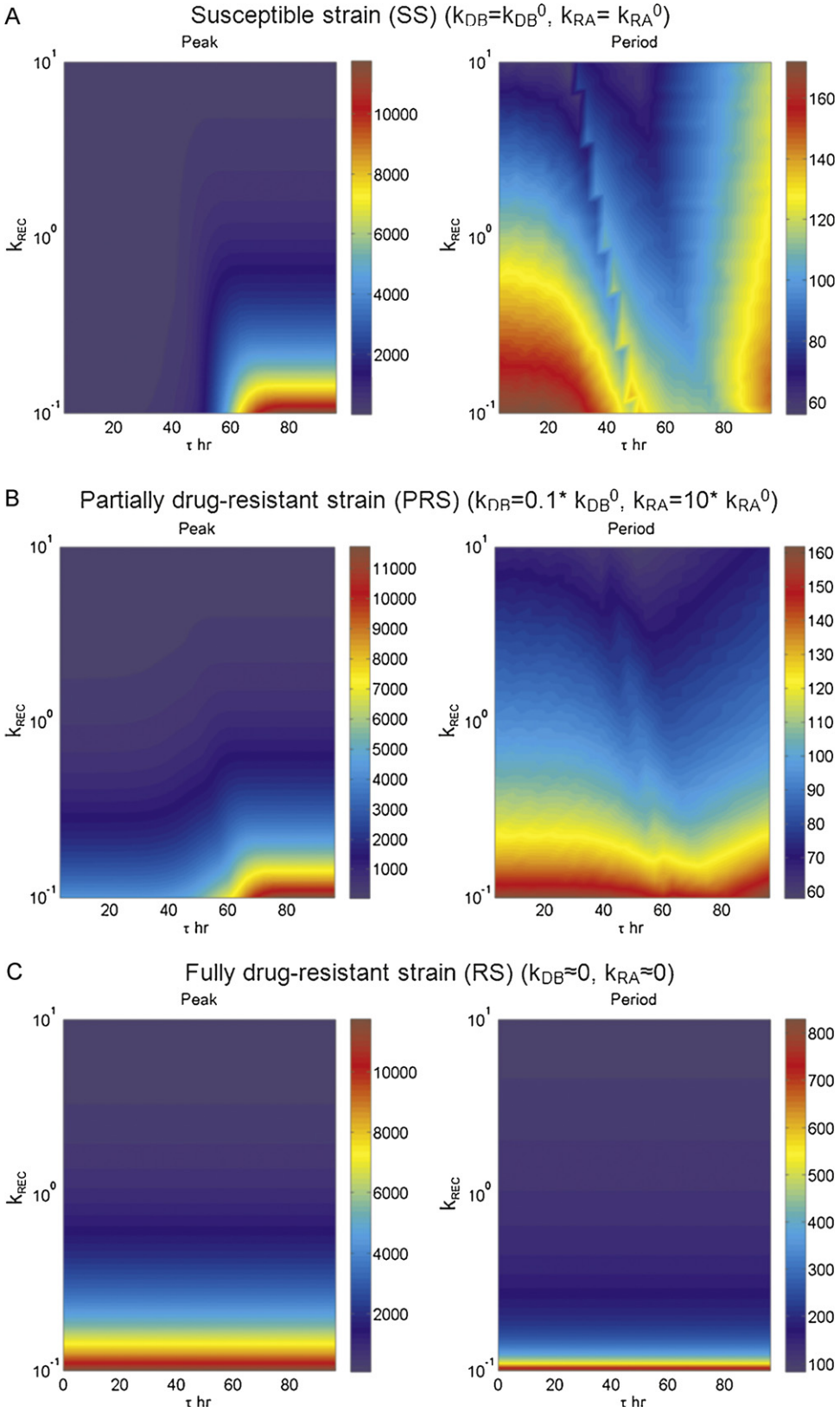

Fig. 6. Predictive simulations: simulated intensity of viral infection peak and the duration of the infection were computed (A) with H1N1 strains that are susceptible to drug; (B) with H1N1 strains with partial resistant to drug; and (C) strains that are fully resistant to drug.

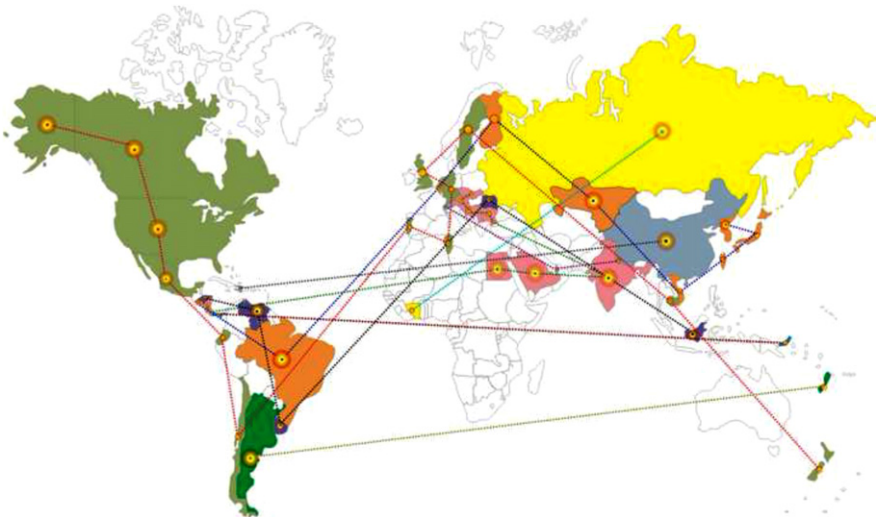

Fig. 7. Geographical distributions of the H1N1 virus based on NA protein sequence similarity. A total of nine groups formed and are represented here by different colors. All representative countries with similar sequences are also linked. (For interpretation of the references to color in this figure legend, the reader is referred to the web version of the article.)

amino acid residues around binding cavity is necessary because of the increasing use of NA inhibitor and to prevent the global distribution of resistant strains.

For most of the samples investigated in the present study, mutations in NA proteins of 2009 pandemic H1N1 strains were clustered adjacent to the zanamivir binding site of the 1918 pandemic H1N1 NA protein, this suggests the resistivity of the virus to the drug by conformational reshuffling of the residues in the binding site. Out of the 34 mutants investigated, mutants isolated form group 2, group 3, group 5, Fiji, Kenya, Montserrat and Nigeria were not found interacting with the drug. Thr157Ala, Asn221Gln, Gly248Lys, Ile349Val and Ile427Val mutations in group 2 and 3, considerably changed the arrangement of residues in binding site that might be the cause of drug ineffectiveness in these strains. Similarly, in group 5, Thr157Ala, Asn221Gln, Gly248Lys, His274Tyr and Ile427Val mutations resulted in complete resistant to zanamivir. Thr157Ala, Asn221Arg, Asn347Asp, Ile349Val in Fiji; Thr157Ala, Gly248Lys, Asn347Asp, Ile349Val, Ile427Val in Kenya; Thr157Ala, Asn221Gln, Ser246Asn, Gln248Lys, His274Tyr, Ile349Val, Ile427Val in Montserrat and Thr157Ala, Asn221Gln, Gly248Lys, His274Tyr, Ile349Val, Ile427Val in Nigeria isolates were also responsible for non interaction of NA

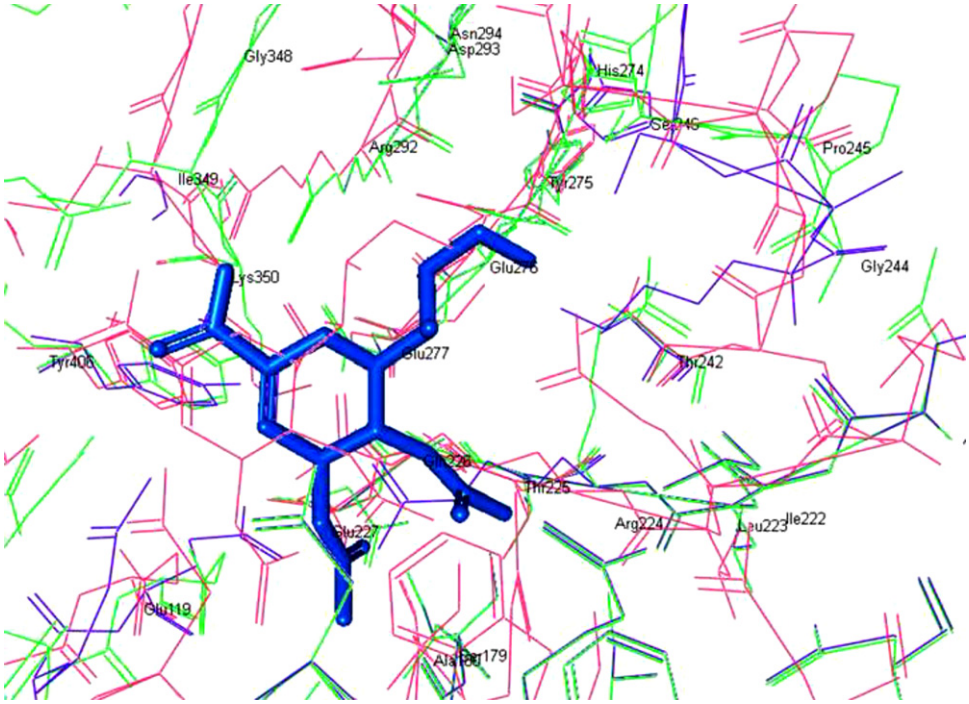

Fig. 8. Structural superimpositions clearly indicate distortion in the binding site of zanamivir (blue) due to the mutations in key amino acid residues. For simplification, only countries in G2 (purple) and G5 (red), where zanamivir did not dock, are superimposed and shown here over 1918 H1N1 NA (PDB id: 1B7E; green color). Amino acid residues participating in the zanamivir interaction are labeled. (For interpretation of the references to color in this figure legend, the reader is referred to the web version of the article.)

with zanamivir. The structure superimposition of key amino acid residues participating in the zanamivir binding site, clearly indicates the impact of these point mutations, resulting in ineffectiveness of the drug (Fig. 8). Docking studies are thus nearly indispensable for analyzing the noticeable changes in zanamivir interactions with mutant models. Variations in Dock-Score suggest the effect of binding site residues and nearby residues mutations on drug binding capacity.

The mathematical model, accounting for the dynamics of RS; PRS and SS, predicts that an early drug administration is required for a patient with weak immune system against infection for all the virus strains, while for a patient with strong immune system, delayed drug administration is possible if infected with susceptible strain. However, an early drug administration is required for infection with partially resistant viral strain.

5. Conclusion

Presently, computational docking and molecular interaction studies play important roles in the rapid assessment and validations of drug candidates. However, to understand the detail insight of disease mechanism and drug resistance, use of mathematical modeling is inevitable. In the present work, we integrated computational modeling and docking techniques with the mathematical model in order to analyze the effectiveness of antiviral therapy in case of H1N1 influenza infection where antigenic drift is a common process to develop the drug resistance. In silico studies are important to immediately raise the alarm against the ineffectiveness of antiviral therapy, if any, and suggest a new way to combat the deadly viral diseases. The mathematical model accounting for the dynamics of the virus with respect to the mutations in NA proteins and their efficacy with antiretroviral drugs can be used in prospective clinical studies, to ascertain whether there are differential long term outcomes and treatment responses between patients infected with the SS, PRS or RS, that were originated due to mutations.

Acknowledgements

OW was supported by the German Research Foundation (DFG). SKG was supported by CSIR NWP-17 project. SKG acknowledge Dr. K.C. Gupta, Director, IITR, Lucknow for his generous support for the work.

Appendix A

Virus populations

$$\frac{dV^{I}}{dt} = k_{syn} \cdot C^{I}(t-\tau_1) - k_{DV} \cdot V^{I} - k_{VA} \cdot V^{I} - k_{DB} \cdot D \cdot V^{I} + k_{RA} \cdot V^{B}$$

$$\frac{dV^{EC}}{dt} = k_{VA} \cdot V^{I} - k_{DV} \cdot V^{EC}$$

$$\frac{dV^{B}}{dt} = k_{DB} \cdot D \cdot V^{I} - k_{RA} \cdot V^{B} - k_{DV} \cdot V^{B}$$

Plasma membrane receptor dynamics

$$\frac{dC^{I}}{dt} = k_{IN} \cdot V^{EC}(t-\tau_2) - k_{FC} \cdot \mathrm{NKC} \cdot C^{I} - k_{APO} \cdot V^{I} \cdot C^{I}$$

$$\frac{d\mathrm{NKC}}{dt} = k_{REC} \cdot C^{I}(t-\tau_3) - k_{DR} \cdot \mathrm{NKC} - k_{VE} \cdot V^{EC} \cdot \mathrm{NKC}$$

Where V^{I} is population of infected cells capable of synthesizing intracellular viruses; V^{EC} is population of extracellular active viruses; V^{B} is population of deactivated viruses after using antiviral drug; C^{I} is population of infected epithelial cells; NKC are population of recruited natural killer cells.

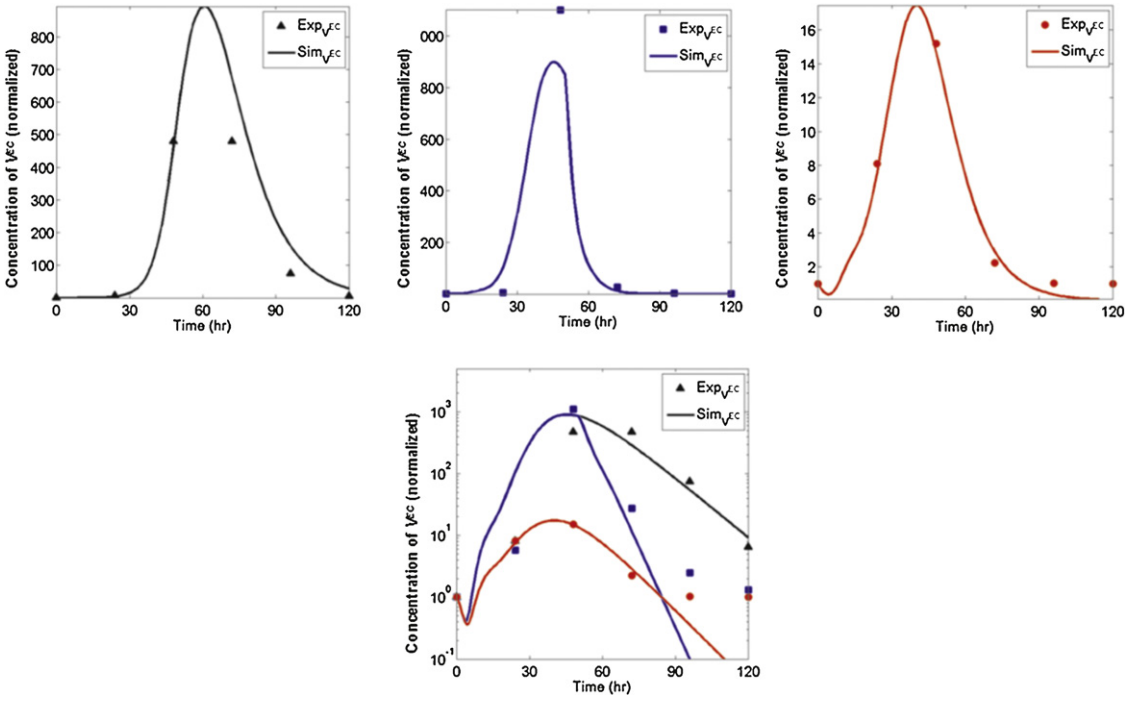

Fig. A1. Time course of data points (dots) versus model predictions (solid lines) for the total viral titer in the three experimental conditions described and essayed in Baccam et al. (2006). Black: no antiviral treatment applied; blue: antiviral treatment applied after 50 h; red: antiviral administered since $t = 0$ h. Top: data fits for the data in linear scale; Bottom: fits for the data in the logarithmic scale. (For interpretation of the references to color in this figure legend, the reader is referred to the web version of the article.)

Different parameters used in ODE are as follows:

k_{syn}: synthesis rate of V^I mediated by C^I
k_{VA}: activation of V^I
k_{RA}: transformation rate from V^B to V^I
k_{FC}: degradation rate of C^I mediated by NKC
k_{REC}: synthesis rate of V^{EC} mediated by C^I
k_{VE}: degradation rate of NKC mediated by V^{EC}
k_{DV}: basal degradation of V^I
k_{DB}: deactivation of V^I by drug (D)
k_{IN}: synthesis rate of C^I mediated by V^{EC}
k_{APO}: degradation rate of C^I mediated by V^I
k_{DR}: basal degradation rate of NKC
D: administration of drugs
τ_1: delay of process depicted by k_{syn}
τ_2: delay of process depicted by k_{IN}
τ_3: delay of process depicted by k_{REC}

Appendix B

The mathematical model to analyze the effectiveness of zanamivir was calibrated using experimental data extracted from Baccam et al. (2006) for three different experimental conditions concerning administration of drugs. Prior to parameter estimation we defined physiologically feasible intervals for some parameters based on published biomedical information (k_{DV} (~6 h), k_{APO} (6–12 h), τ_1 and τ_3 (~6 h) and τ_2 (6–12 h)) and set the rest parameters in a free interval. Parameter estimation was performed using parameter estimation functions implemented in SBtoolbox 2 (Schmidt and Jirstrand, 2006) for Matlab (Mathworks, MA) running in a standard PC under Windows XP. The computing time was in the order of minutes for each parameter estimation round. Estimated values for the parameters are listed in the table below:

Model parameter values.

Parameter	Value	Parameter	Value
k_{syn}	1.04164×10^{-5} h^{-1}	k_{DV}	0.3 h^{-1}
k_{VA}	0.00628761 h^{-1}	k_{DB}	1.74233 h^{-1}
k_{RA}	0.000343459 h^{-1}	k_{IN}	804106 h^{-1}
k_{FC}	4.37084×10^{-5} h^{-1}	k_{APO}	0.0478 h^{-1} (6–12 h)
k_{REC}	6.67951×10^{-5} h^{-1}	k_{DR}	1.10021×10^{-5} h^{-1}
k_{VE}	1.00015×10^{-5} h^{-1}	τ_1	6 h
τ_2	12–48 h	τ_3	6 h

Appendix Fig. A1 shows the results of the data fitting problem for the best solution. We notice that the model predictions are in good agreement with the experimental data. However, the fitting is not perfect, which we think relate to (a) the structural simplicity of the derived model and (b) the intrinsic variability in the experimental data used.

To further obtain insight into the confidence in the estimated parameters and the correlations between them, we randomly uniformly perturbed the parameter values in the interval from tenth to ten folder of their estimated values $[10^{-1}, 10^{1}]$ and use the generated parameter values to repeat the parameter estimation for 2000 times according to the procedure described in SBtoolbox2 (www.sbtoolbox2.org). Among these 2000 estimations we sort out different combinations of the parameters by using which the model can reach around the minimum cost function. Based on the these different combinations of parameter values, Appendix Fig. A2 plots out the absolute correlation matrix for the model parameters, in which 1 represents the strongest correlation between a pair of parameters and

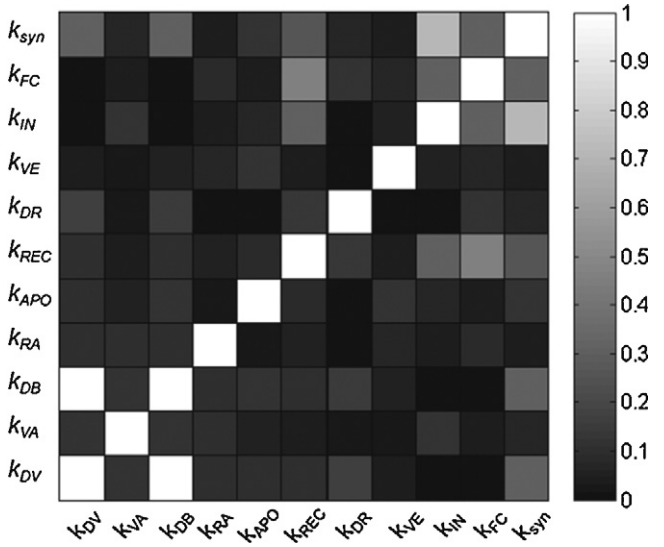

Fig. A2. Correlation matrix for the model parameters. Here, 1 represents the strongest correlation between a pair of parameters (color white), while 0 represents no correlation between them (color black).

0 represents no correlation between them. As we can see, the model performs properly concerning parameter correlation and the parameters are poorly correlated. The exception is the couple of parameters k_{DV} and k_{DB}, which shows correlation. We notice that this has no effect in the performance of the model given that the value of k_{DV} was assigned prior to estimation of the other parameters and has therefore no influence in the identifiability of other model parameters.

Appendix C. Supplementary data

Supplementary data associated with this article can be found, in the online version, at doi:10.1016/j.meegid.2011.03.018.

References

Alexander, M.E., Moghadas, S.M., Röst, G., Wu, J., 2008. A delay differential model for pandemic influenza with antiviral treatment. Bull. Math. Biol. 70, 382–397.
Altmuller, A., Kunerl, M., Muller, K., Hinshaw, V.S., Fitch, W.M., Scholtissek, C., 1992. Genetic relatedness of the nucleoprotein (NP) of recent swine, turkey, and human influenza A virus (H1N1) isolates. Virus Res. 22, 79–87.
Baccam, P., Beauchemin, C., Macken, C.A., Hayden, F.G., Perelson, A.S., 2006. Kinetics of influenza A virus infection in humans. J. Virol. 80, 7590–7599.
Barnett, J.M., Cadman, A., Gor, D., Dempsey, M., Walters, M., Candlin, A., Tisdale, M., Morley, P.J., Owens, I.J., Fenton, R.J., Lewis, A.P., Claas, E.C.J., Rimmelzwaan, G.F., De Groot, R., Osterhaus, A.D.M.E., 2000. Zanamivir susceptibility monitoring and characterization of influenza virus clinical isolates obtained during phase II clinical efficacy studies. Antimicrob. Agents Chemother. 44, 78–87.
Beauchemin, C., Samuel, J., Tuszynski, J., 2005. A simple cellular automaton model for influenza A viral infections. J. Theor. Biol. 232, 223–234.
Bocharov, G.A., Romanyukha, A.A., 1994. Mathematical model of antiviral immune response. III. Influenza A virus infection. J. Theor. Biol. 167, 323–360.
Bright, R.A., Shay, D.K., Shu, B., Cox, N.J., Klimov, A.I., 2006. Adamantane resistance among influenza A viruses isolated early during the 2005–2006 influenza season in the United States. Jama-J. Am. Med. Assoc. 295, 891–894.
Brown, I.H., 2000. The epidemiology and evolution of influenza viruses in pigs. Veter. Microbiol. 74, 29–46.
Burmeister, W.P., Daniels, R.S., Dayan, S., Gagnon, J., Cusack, S., Ruigrok, R.W.H., 1991. Sequence and crystallization of influenza-virus B/Beijing/1/87 neuraminidase. Virology 180, 266–272.
Colman, P.M., 1999. A novel approach to antiviral therapy for influenza. J. Antimicrob. Chemother. 44, 17–22.
de Jong, J.C., Smith, D.J., Lapedes, A.S., Donatelli, I., Campitelli, L., Barigazzi, G., Van Reeth, K., Jones, T.C., Rimmelzwaan, G.F., Osterhaus, A.D.M.E., Fouchier, R.A.M., 2007. Antigenic and genetic evolution of swine influenza A (H3N2) viruses in Europe. J. Virol. 81, 4315–4322.
Du, Q.S., Wang, S.Q., Huang, R.B., Chou, K.C., 2010. Computational 3D structures of drug-targeting proteins in the 2009-H1N1 influenza A virus. Chem. Phys. Lett. 485, 191–195.

Eramian, D., Shen, M.Y., Devos, D., Melo, F., Sali, A., Marti-Renom, M.A., 2006. A composite score for predicting errors in protein structure models. Prot. Sci. 15, 1653–1666.

Ferraris, O., Kessler, N., Lina, B., 2005. Sensitivity performed of influenza viruses to zanamivir and oseltamivir: a study on viruses circulating in France prior to the introduction of neuraminidase inhibitors in clinical practice. Antivir. Res. 68, 43–48.

Feyfant, E., Sali, A., Fiser, A., 2007. Modeling mutations in protein structures. Prot. Sci. 16, 2030–2041.

Gehlhaar, D.K., Verkhivker, G.M., Rejto, P.A., Sherman, C.J., Fogel, D.B., Fogel, L.J., Freer, S.T., 1995. Molecular recognition of the inhibitor AG-1343 by HIV-1 protease: conformationally flexible docking by evolutionary programming. Chem. Biol. 2, 317–324.

Gehlhaar, D., Bouzida, D., Rejto, P., 1999. Reduced dimensionality in ligand–protein structure prediction: covalent inhibitors of serine proteases and design of sitedirected combinatorial libraries. In: Parrill, L., Rami Reddy, M. (Eds.), Rational Drug Design: Novel Methodology and Practical Applications (ACS Symposium Series). American Chemical Society, Washington, DC, pp. 292–311.

Gupta, S.K., Srivastava, M., Akhoon, B.A., Smita, S., Schmitz, U., Wolkenhauer, O., Vera, J., Gupta, S.K., 2010. Identification of immunogenic consensus T-cell epitopes globally distributed influenza-A H1N1 neuraminidase. Infect. Genet. Evol., doi:10.1016/j.meegid.2010.10.013.

Hurt, A.C., Holien, J.K., Parker, M., Kelso, A., Barr, I.G., 2009. Zanamivir-resistant influenza viruses with a novel neuraminidase mutation. J. Virol. 83 (20), 10366–10373.

Ives, J.A., Carr, J.A., Mendel, D.B., Tai, C.Y., Lambkin, R., Kelly, L., Oxford, J.S., Hayden, F.G., Roberts, N.A., 2002. The H274Y mutation in the influenza A/H1N1 neuraminidase active site following oseltamivir phosphate treatment leave virus severely compromised both in vitro and in vivo. Antivir. Res. 55 (2), 307–317.

Jain, A.N., 1996. Scoring noncovalent protein-ligand interactions: a continuous differentiable function tuned to compute binding affinities. J. Comput. Aided Mol. Des. 10, 427–440.

Krammer, A., Kirchhoff, P.D., Jiang, X., Venkatachalam, C.M., Waldman, M., 2005. LigScore: a novel scoring function for predicting binding affinities. J. Mol. Graphics Model. 23, 395–407.

Larkin, M.A., Blackshields, G., Brown, N.P., Chenna, R., McGettigan, P.A., McWilliam, H., Valentin, F., Wallace, I.M., Wilm, A., Lopez, R., Thompson, J.D., Gibson, T.J., Higgins, D.G., 2007. Clustal W and clustal X version 2.0. Bioinformatics 23, 2947–2948.

McSharry, J.J., McDonough, A.C., Olson, B.A., Drusano, G.L., 2004. Phenotypic drug susceptibility assay for influenza virus neuraminidase inhibitors. Clin. Diagnos. Lab. Immunol. 11, 21–28.

Mesecar, A.D., Ratia, K., 2008. Viral destruction of cell surface receptors. In: Proceedings of the National Academy of Sciences of the United States of America, 105, 8807–8808.

Monto, A.S., Moult, A.B., Sharp, S.J., 2000. Effect of zanamivir on duration and resolution of influenza symptoms. Clin. Ther. 22, 1294.

Muegge, I., Martin, Y.C., 1999. A general and fast scoring function for protein ligand interactions: a simplified potential approach. J. Med. Chem. 42, 791–804.

Olsen, C.W., 2002. The emergence of novel swine influenza viruses in North America. Virus Res. 85, 199–210.

Rice, P., Longden, I., Bleasby, A., 2000. EMBOSS: the European molecular biology open software suite. Trends Genet. 16, 276–277.

Schmidt, H., Jirstrand, M., 2006. Systems Biology Toolbox for MATLAB: a computational platform for research in systems biology. Bioinformatics 22, 514–515.

Scholtissek, C., Ludwig, S., Fitch, W.M., 1993. Analysis of influenza-A virus nucleoproteins for the assessment of molecular-genetic mechanisms leading to new phylogenetic virus lineages. Arch. Virol. 131, 237–250.

Schweiger, B., Zadow, I., Heckler, R., 2002. Antigenic drift and variability of influenza viruses. Med. Microbiol. Immunol. 191, 133–138.

Shen, M.Y., Sali, A., 2006. Statistical potential for assessment and prediction of protein structures. Prot. Sci. 15, 2507–2524.

Taylor, N.R., Vonitzstein, M., 1994. Molecular modeling studies on ligand-binding to sialidase from influenza-virus and the mechanism of catalysis. J. Med. Chem. 37, 616–624.

Wang, M.Z., Tai, C.Y., Mendel, D.B., 2002. Mechanism by which mutations at His274 alter sensitivity of influenza A virus N1 neuraminidase to oseltamivir carboxylate and zanamivir. Antimicrob. Agents Chemother. 46 (12), 3809–3816.

Wang, S.Q., Du, Q.S., Huang, R.B., Zhang, D.W., Chou, K.C., 2009. Insights from investigating the interaction of oseltamivir (Tamiflu) with neuraminidase of the 2009 H1N1 swine flu virus. Biochem. Biophys. Res. Commun. 386 (3), 432–436.

Wang, T.T., Palese, P., 2009. Unraveling the mystery of swine influenza virus. Cell 137, 983–985.

Wang, Y.T., Chan, C.H., Su, Z.Y., Chen, C.L., 2010. Homology modeling, docking, and molecular dynamics reveal HR1039 as a potent inhibitor of 2009 A(H1N1) influenza neuraminidase. Biophys. Chem. 147 (1–2), 74–80.

Waterhouse, A.M., Procter, J.B., Martin, D.M.A., Clamp, M., Barton, G.J., 2009. Jalview Version 2-a multiple sequence alignment editor and analysis workbench. Bioinformatics 25, 1189–1191.

Webby, R.J., Swenson, S.L., Krauss, S.L., Gerrish, P.J., Goyal, S.M., Webster, R.G., 2000. Evolution of swine H3N2 influenza viruses in the United States. J. Virol. 74, 8243–8251.

Webster, R.G., Bean, W.J., Gorman, O.T., Chambers, T.M., Kawaoka, Y., 1992. Evolution and ecology of influenza-A viruses. Microbiol. Rev. 56, 152–179.

Xu, X.J., Zhu, X.Y., Dwek, R.A., Stevens, J., Wilson, I.A., 2008. Structural characterization of the 1918 influenza virus H1N1 neuraminidase. J. Virol. 82, 10493–10501.